JPE 16-3-33

http://dx.doi.org/10.6113/JPE.2016.16.3.1163
ISSN(Print): 1598-2092 / ISSN(Online): 2093-4718

New Techniques for Impedance Characteristics Measurement of Islanded Microgrid based on Stability Analysis

Lixiang Hou†, Fang Zhuo*, and Hongtao Shi*

State Key Laboratory of Electrical Insulation and Power Equipment, Xi'an Jiaotong University, China

Abstract

In recent years, microgrids have been the focus of considerable attention in distributed energy distribution. Microgrids contain a large number of power electronic devices that can potentially cause negative impedance instability. Harmonic impedance is an important tool to analyze stability and power quality of microgrids. Harmonic impedance can also be used in harmonic source localization. Precise measurement of microgrid impedance and analysis of system stability with impedances are essential to increase stability. In this study, we introduce a new square wave current injection method for impedance measurement and stability analysis. First, three stability criteria based on impedance parameters are presented. Then, we present a new impedance measurement method for microgrids based on square wave current injection. By injecting an unbalanced line-to-line current between two lines of the AC system, the method determines all impedance information in the traditional synchronous reference frame *d*–*q* model. Finally, the microgrid impedances of each part and the overall microgrid are calculated to verify the measurement results. In the experiments, a simulation model of a three-phase AC microgrid is developed using PSCAD, and the AC system harmonic impedance measuring device is developed.

Key words: Current injection, Harmonic impedance, Impedance, Impedance measurement, Microgrid

I. INTRODUCTION

Microgrids are localized small-scale grids connected to the centralized macrogrids and can strengthen grid resilience and help mitigate grid disturbances. In recent years, microgrids have been the focus of considerable attention in distributed energy systems. Many studies have been dedicated to new applications of small-power-rate distributed power generators [1]-[6]. Compared with macrogrids, microgrids have smaller capacity but higher proportion of renewable energy, which is used by a large number of power electronic devices. Power electronic devices are prone to negative impedance instability given the constant-power nature of the individual components [7]-[13]. When designing and building power systems that contain many power electronic switching sources and loads, system integrators must consider frequency-dependent impedance characteristics to ensure system stability. Guerrero et al. [6] analyzed the selection of droop gains to ensure microgrid stability. Liu et al. [9] and Xiao et al. [10] indicated that a large droop gain will result in system instability using a small signal model. Pogaku et al. [2] indicated that instabilities can be avoided by modifying the power electronic control mode. However, these stability analysis methods need to model the system, which is difficult to use in practice. Other studies defined the admittance space criteria based on a DC interface that can be used to design system components. Middlebrook [13] analyzed system stability through impedance parameters, whereas Liu et al. [14], Sudhoff et al. [15], and Sun [16] further deduced the criterion to make it more accurate. A common problem of these methods is that a system phase–frequency curve is needed to use the stability criteria. However, obtaining an accurate phase–frequency curve in practical settings is difficult. This difficulty is due to harmonic current decay becoming a serious problem particularly in high frequency. Moreover, the amplitude of impedance is close to zero and the impedance phase is the ratio of real and imaginary parts.

Manuscript received Jul. 29, 2015; accepted Dec. 7, 2015
Recommended for publication by Associate Editor Il-Yop Chung.
†Corresponding Author:hawkhou666@163.com
Tel: +86-159-9169-2578, Fax: +89-29-8266-5223, Xi'an Jiaotong Univ.
*State Key Laboratory of Electrical Insulation and Power Equipment, Xi'an Jiaotong University, China

Therefore, small disturbances in the impedance phase can have a significant effect on the phase–frequency curve.

Many existing impedance measurement methods are based on measuring the voltage and current disturbances at the operating point. The impedance measurement methods can be classified into three categories: (1) utilizing the harmonic current from existing nonlinear loads; (2) introducing auxiliary switching elements, such as a shunt capacitor, reactor, or transformer; and (3) directly injecting harmonic currents with additional devices. Xiao et al. [17], Yang et al. [18], and Bridgeman et al. [19] theoretically analyzed the first method. The second method is introduced in the studies of Feng et al. [20] and Feng and Lee [21], in which the capacitor and sub-circuit are switched into a microgrid to measure system impedance, respectively. The disadvantages of these methods are that the injected harmonic current cannot be accurately controlled and does not cover all frequency ranges, which reduces measurement accuracy. Hou et al. [22], [23] and Shi et al. [24] introduced a method directly injecting harmonic currents with three-phase full-bridge circuits. The problem in the third method is that it requires injection of perturbation signals to the system one frequency at a time. Multiple tests must be repeatedly performed, which take a long online time to complete, to obtain the impedance characteristics over a wide frequency range. The operating point of the system may vary during the prolonged test procedure, which can lead to inconsistencies in the measured system impedance characteristics. The three methods need two different injection angles φ_{inj} for each injection frequency of interest, which means harmonic current must be injected twice at the same frequency.

This paper is organized as follows: In Section 2, the theoretical impedance of microgrids is calculated. Section 3 focuses on three stability criteria based on the impedance parameters. The proposed stability criterion only needs system amplitude–frequency curve, which is more convenient in practical applications. In Section 4, a new method for measuring microgrid harmonic impedance is introduced. By injecting an unbalanced line-to-line current between two lines of the AC system, all impedance information in the traditional synchronous reference frame *d–q* model can be determined. The proposed method requires only one injection and measurement process. This method can not only be applied to the AC system but can also be applied to the DC system. Finally, the experimental results show the effectiveness and advantages of the proposed method.

II. The Harmonic Impedance Calculation

For a known system, the output impedance of an inverter can be calculated by substituting the parameters into the model of output impedance. The theoretical value can be compared with the measurement value of impedance to validate the effectiveness of the proposed impedance measurement method. The simplest microgrid structure is taken as an example (Fig. 1).

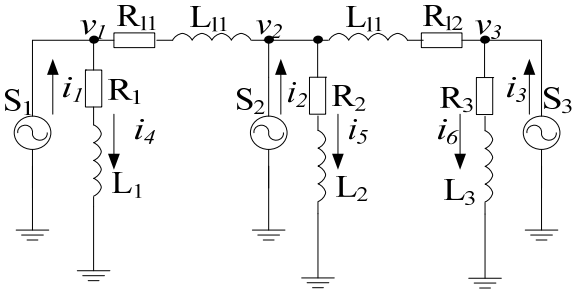

Fig. 1. Equivalent circuit of the microgrid.

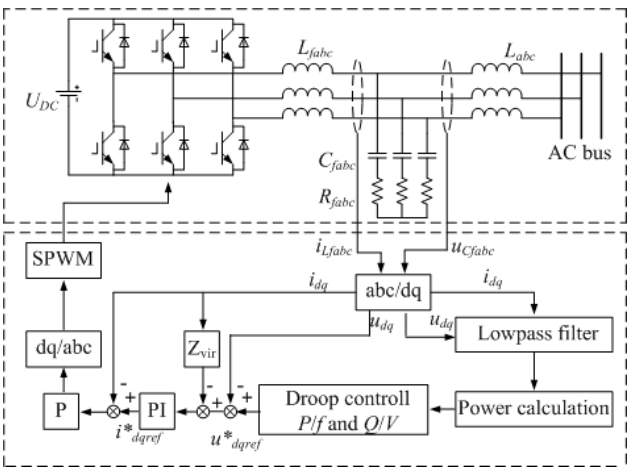

Fig. 2. Structure of voltage source inverter.

In Fig. 1, S1, S2, and S3 represent three distributed power generators, which are connected to a microgrid through inverters; R1, L1, L2, R2, and R3, L3 imply common loads; and Rl1 and Ll1 indicate bus line impedances. System impedances are significantly affected by the inverters.

A. Harmonic Impedance of Voltage Source Inverter

The microgrid investigated in this study operates in islanding mode, and all the inverters are controlled by droop control strategy. All inverters are controlled to be voltage sources; active and reactive power of loads will be shared by all inverters by regulating the amplitude and frequency of the output voltage of inverters, respectively. In [25]-[27], virtual impedance is added to decouple the droop control for active and reactive power. Generally, the inverter control system has four control loops, namely, droop control loop, virtual impedance loop, voltage control loop, and current control loop (Fig. 2).

As illustrated in Fig. 2, all control loops are established in synchronous *d–q* coordinate. Therefore, the small signal model of the inverter can be developed in the synchronous *d–q* coordinate (Fig. 3).

$G_v(s)$ and $G_i(s)$ are transfer functions of the voltage controller and current controller, respectively. KPWM is the equivalent transfer function of the PWM link and H bridge,

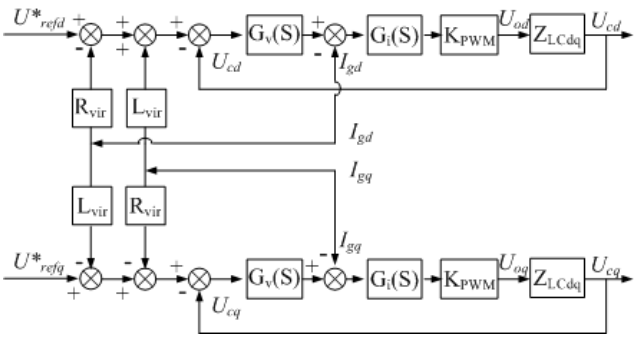

Fig. 3. Control diagram of the voltage source inverter.

TABLE I
PARAMETERS OF THE SAMPLE INVERTER

Parameter	Value	Parameter	Value
K_{vp}	0.052	K_{ip}	0.025
K_{vi}	20	K_{ii}	100
U_{DC}	200 V	R_f	1 Ω
L_f	0.72 mH	R_v	1 Ω
C_f	30 μF	L_v	10 mH

which is approximately equal to half of the DC voltage. In practical control systems of the inverter, this step is realized in the *a–b–c* coordinate. The transfer function of the PWM link and H bridge is converted to the synchronous *d–q* coordinate to obtain impedance in the synchronous *d–q* coordinate. Z_{LCdq} is the equivalent transfer function of the LC filter of the inverter in the synchronous *d–q* coordinate, which can be obtained in the following discussion.

In the *a–b–c* coordinate, the voltage and current of the filter satisfy the following equations:

$$L_f \cdot \frac{d}{dt}\begin{bmatrix} i_{La} \\ i_{Lb} \\ i_{Lc} \end{bmatrix} = \begin{bmatrix} u_{oa} \\ u_{ob} \\ u_{oc} \end{bmatrix} - \begin{bmatrix} u_{ca} \\ u_{cb} \\ u_{cc} \end{bmatrix}, \quad (1)$$

$$\begin{bmatrix} i_{ca} \\ i_{cb} \\ i_{cc} \end{bmatrix} = C_f \cdot \frac{d}{dt}\left(\begin{bmatrix} u_{ca} \\ u_{cb} \\ u_{cc} \end{bmatrix} - R_f \cdot \begin{bmatrix} i_{ca} \\ i_{cb} \\ i_{cc} \end{bmatrix} \right), \quad (2)$$

$$\begin{bmatrix} i_{ga} \\ i_{gb} \\ i_{gc} \end{bmatrix} = \begin{bmatrix} i_{La} \\ i_{Lb} \\ i_{Lc} \end{bmatrix} - \begin{bmatrix} i_{ca} \\ i_{cb} \\ i_{cc} \end{bmatrix}, \quad (3)$$

where i_{Labc} is the inductive currents, i_{gabc} is the grid-connected currents, u_{cabc} is the capacitive voltages, and u_{oabc} is the output voltages of the inverter. The equations are transferred to the frequency domain using Laplace transformation. Through proper simplification, constraint equations in the synchronous *d–q* coordinate can be obtained as follows:

$$\begin{bmatrix} u_{od} \\ u_{oq} \end{bmatrix} = \begin{bmatrix} R & T \\ -T & R \end{bmatrix} \cdot \begin{bmatrix} u_{gd} \\ u_{gq} \end{bmatrix} + \begin{bmatrix} s \cdot L_f & \omega_0 \cdot L_f \\ -\omega_0 \cdot L_f & s \cdot L_f \end{bmatrix} \cdot \begin{bmatrix} i_{gd} \\ i_{gq} \end{bmatrix}, \quad (4)$$

where:

$$R = \frac{C_f L_f \left[2\omega_0^2 R_f C_f + \left(s^2 + \omega_0^2 \right) \left(1 + sR_f C_f \right) \right]}{\left(1 + sR_f C_f \right)^2 + \omega_0^2 {R_f}^2 {C_f}^2} + 1,$$

$$T = \frac{R_f {C_f}^2 L_f \left(s^2 + \omega_0^2 \right) + \omega_0 s C_f \left(L_f + 1 \right)}{\left(1 + sR_f C_f \right)^2 + \omega_0^2 {R_f}^2 {C_f}^2}.$$

From Fig. 3, the transfer function between the output voltage of the inverter and the reference voltage can be established as follows:

$$\begin{bmatrix} u_{od}(\mathrm{s}) \\ u_{oq}(\mathrm{s}) \end{bmatrix} = A \cdot \begin{bmatrix} U_{refd(\mathrm{s})} \\ U_{refq(\mathrm{s})} \end{bmatrix} - A \cdot \begin{bmatrix} u_{cd(\mathrm{s})} \\ u_{cq(\mathrm{s})} \end{bmatrix} + \begin{bmatrix} -C & B \\ -B & -C \end{bmatrix} \cdot \begin{bmatrix} i_{gd}(\mathrm{s}) \\ i_{gq}(\mathrm{s}) \end{bmatrix}, \quad (5)$$

where:

$$A = G_v(\mathrm{s}) \cdot \mathrm{G}_i(\mathrm{s}) \cdot K_{PWM}, \quad B = \omega_0 \cdot L_{vir} \cdot A,$$

$$C = \mathrm{G}_i(\mathrm{s}) \cdot K_{PWM} \cdot (1 + R_{vir} \cdot G_v(\mathrm{s})).$$

By combining Eqs. (4) and (5), the impedance matrix model of the inverter in the synchronous *d–q* coordinate can be obtained as follows:

$$\begin{bmatrix} Z_{dd}(\mathrm{s}) & Z_{dq}(\mathrm{s}) \\ Z_{qd}(\mathrm{s}) & Z_{qq}(\mathrm{s}) \end{bmatrix} = \frac{1}{H} \begin{bmatrix} L & Q \\ -Q & L \end{bmatrix}, \quad (6)$$

where:

$$H = R + A + \frac{T^2}{R + A}, \quad L = C + sL_f - \frac{T(B - \omega_0 L_f)}{R + A},$$

$$Q = \omega_0 L_f - B - \frac{T(C - \omega_0 L_f)}{R + A}.$$

To calculate the output impedance of the inverter, the parameters of a sample inverter are shown in Table I.

B. Load Harmonic Impedance

If the system load is Y-connected and is three-phase symmetrical, then the corresponding load impedance in each phase can be expressed as follows:

$$Z = R + jX = R + j\omega L, \quad (7)$$

$$i_a + i_b + i_c = 0, \quad (8)$$

$$i_a \bullet (R + jX) - i_b \bullet (R + jX) = u_{ab}, \quad (9)$$

$$i_b \bullet (R + jX) - i_c \bullet (R + jX) = u_{bc}. \quad (10)$$

From the results of Eqs. (8) to (10), the following expressions can be obtained:

$$i_a = \frac{1}{3(R + jX)} (2u_a - u_b - u_c), \quad (11)$$

$$i_b = \frac{1}{3(R + jX)} (2u_b - u_a - u_c), \quad (12)$$

$$i_c = \frac{1}{3(R+jX)}(2u_c - u_b - u_a). \quad (13)$$

By converting Eqs. (11) to (13) to matrix form, the following expressions can be obtained:

$$\begin{bmatrix} i_a \\ i_b \\ i_c \end{bmatrix} = \frac{1}{3(R+jX)} \begin{bmatrix} 2 & -1 & -1 \\ -1 & 2 & -1 \\ -1 & -1 & 2 \end{bmatrix} \begin{bmatrix} v_a \\ v_b \\ v_c \end{bmatrix} \quad (14)$$

and

$$Y_{abc} = \frac{1}{3(R+jX)} \begin{bmatrix} 2 & -1 & -1 \\ -1 & 2 & -1 \\ -1 & -1 & 2 \end{bmatrix}. \quad (15)$$

The sequence admittance matrix can be expressed as follows:

$$Y_{012} = \frac{3}{R+jX} \begin{bmatrix} 0 & 0 & 0 \\ 0 & 1 & 0 \\ 0 & 0 & 1 \end{bmatrix}. \quad (16)$$

The sequence impedance matrix can be expressed as follows:

$$Z_{012} = (R+jX) \begin{bmatrix} \infty & 0 & 0 \\ 0 & 1 & 0 \\ 0 & 0 & 1 \end{bmatrix}. \quad (17)$$

Thus, the sequence harmonic impedance matrix of load can be expressed as follows:

$$Z_{012}(h) = (R+jL\omega h) \begin{bmatrix} \infty & 0 & 0 \\ 0 & 1 & 0 \\ 0 & 0 & 1 \end{bmatrix}. \quad (18)$$

C. Microgrid System Impedance

The previous sections introduced the harmonic impedance calculating method for each part of the microgrid. With this information, we can obtain the harmonic impedance for the entire microgrid.

According to Fig. 1, each inverter is controlled as voltage source when the microgrid works in islanding mode. By defining $Y_{S1}(h)$, $Y_{S2}(h)$, and $Y_{S3}(h)$ as output harmonic admittance of the three inverters, $Y_{S1}(h)$ could be expressed in Eq. (19) through Eq. (6):

$$Y_{S1} = \frac{1}{Z_{I1}(h)} = \frac{L_{f1}C_f(j\omega h)^3 + C_f K_{ip}\frac{U_{DC}}{2}(j\omega h)^2 + (K_{ip}K_{ip}\frac{U_{DC}}{2}+1)(j\omega h) + K_{ii}K_{ip}\frac{U_{DC}}{2}}{L_{f1}L_{f2}C_f(j\omega h)^4 + C_f L_{f2}K_{ip}\frac{U_{DC}}{2}(j\omega h)^3 + (L_{f1}+L_{f2})(j\omega h)^2}. \quad (19)$$

In addition, assuming that two loads are Y-connected and are three-phase symmetrical, the harmonic impedances of load could be obtained as follows:

$$Y_{L1}(h) = Y_{L2}(h) = \frac{1}{Z_{L1}(h)} = \frac{1}{R_1 + jL_1\omega h}. \quad (20)$$

From Eqs. (19) and (20), microgrid system impedance could be calculated.

III. Stability Criteria of the Microgrid

For stability analysis, most studies focus on the impedance/admittance method, which involves examining the Nyquist contour of the product of the source impedance and load admittance in a DC system. In recent years, based on the impedance/admittance method, a variety of stability criteria and design approaches for DC and AC systems have been proposed. The common problem of these methods is their need for system phase–frequency curves. However, obtaining an accurate phase–frequency curve in practical application is difficult. This difficulty is due to harmonic current decay becoming a serious problem particularly in high frequency. Moreover, the amplitude is close to zero and the impedance phase angle parameter is the ratio of real and imaginary parts. Therefore, a small deviation can have a significant effect on the phase–frequency curve. Therefore, this study proposes three stability criteria that are based on the impedance parameters. The proposed stability criterion only needs the system amplitude–frequency curve, which is more feasible in practical applications.

Microgrid stability could be assessed by source and load impedances. For the example system shown in Fig. 1, an AC boundary was selected in the AC bus, which defines the source and load. In the steady state, source impedances are related to voltages and currents, as follows:

$$\begin{bmatrix} V_q \\ V_d \end{bmatrix} = \begin{bmatrix} Z_{qqS} & Z_{qdS} \\ Z_{dqS} & Z_{qqS} \end{bmatrix} = \begin{bmatrix} I_{qS} \\ I_{dS} \end{bmatrix}. \quad (21)$$

In the load, admittance can be expressed in terms of voltages and currents, as follows:

$$\begin{bmatrix} I_{qL} \\ I_{dL} \end{bmatrix} = \begin{bmatrix} Y_{qqL} & Y_{qdL} \\ Y_{dqL} & Y_{qqL} \end{bmatrix} = \begin{bmatrix} V_q \\ V_d \end{bmatrix}. \quad (22)$$

If $\|X\| = \sqrt{X^H X}$, then

$$\sigma(\omega) < 1 \quad -\infty < \omega < +\infty, \quad (23)$$

where σ is the largest singular value of $Z_S Y_L$ and is frequency-dependent. If the induced norm of $Z_S Y_L$ is restricted to be less than unity at all frequencies and if $A = Z_s Y_L$ is normal, then each singular value of A denoted by σ_i can be expressed as follows:

$$\sigma_i(\omega) = \left|\lambda_i(\omega)\right|. \quad (24)$$

If the largest singular value is less than one, then

$$\prod_i \lambda_i(\omega) = \det(Z_S Y_L) < 1 \quad -\infty < \omega < +\infty. \quad (25)$$

The characteristic loci will lie within the unit circle. Furthermore, by Cauchy's inequality,

$$\left\|Z_S Y_L\right\|_M < 1/2 . \quad (26)$$

If $\|Z_s\|\,\|Y_L\| < 1$, then the characteristic loci will not encircle (−1, j_0). The system meets the following formula, which can maintain stability:

$$\sigma\left(Z_S,\omega\right)\sigma\left(Y_L,\omega\right) < 1 . \quad (27)$$

Another stability criterion for the AC system could be derived from the entries of matrix $Z_S Y_L$. In the derivation process, Gershgorin's theorem is mainly used. According to Gershgorin's theorem, if a complex matrix Z is $m \times m$, then the eigenvalues range of the matrix inner circle, in which Z_{ij} is the center and R_i is the radius.

$$R_i = \sum_{j=1, j\neq i}^{n} \left|Z_{ij}\right|, i = 1,\ldots m \quad (28)$$

If the largest entry of $Z_S Y_L$ in magnitude is less than half at all frequencies, then the eigenvalues of $Z_S Y_L$ will be within the unit circle. A new norm $\|\ \|_M$ could be defined as follows:

$$\left\|Z_S Y_L\right\|_M = MAX\left(\left|A_{11}\right|,\left|A_{12}\right|,\left|A_{21}\right|,\left|A_{22}\right|\right). \quad (29)$$

If the system satisfies $\|Z_S Y_L\|_M < 1/2$ within all frequencies, then the characteristic loci will not encircle the critical point (−1, j_0) and the system remains stable.

Given that the previous condition is in a coupled form, how changes in the individual entries of Z_S or Y_L would affect system stability is unclear. Z_S and Y_L are also measured. After deriving the matrix algebra, decoupling this norm into a condition based on the individual norms of Z_S and Y_L is possible.

$$Z_S Y_L = \begin{pmatrix} a_1 & b_1 \\ c_1 & d_1 \end{pmatrix}\begin{pmatrix} a_2 & b_2 \\ c_2 & d_2 \end{pmatrix} \quad (30)$$

Then, a sufficient and necessary condition for maintaining stability can be expressed as follows:

$$\left|a_1 a_2 + b_1 c_2\right| < 1/2, \quad (31)$$

$$\left|c_1 a_2 + d_1 c_2\right| < 1/2, \quad (32)$$

$$\left|a_1 b_2 + b_1 d_2\right| < 1/2, \quad (33)$$

$$\left|c_1 b_2 + d_1 d_2\right| < 1/2 . \quad (34)$$

Using Cauchy's inequality, the following expressions can be obtained:

$$\left|a_1\right|\left|a_2\right| + \left|b_1\right|\left|c_2\right| < 1/2, \quad (35)$$

$$\left|c_1\right|\left|a_2\right| + \left|d_1\right|\left|c_2\right| < 1/2, \quad (36)$$

$$\left|a_1\right|\left|b_2\right| + \left|b_1\right|\left|d_2\right| < 1/2, \quad (37)$$

$$\left|c_1\right|\left|b_2\right| + \left|d_1\right|\left|d_2\right| < 1/2 . \quad (38)$$

The system will be stable if the previous condition is true. This characteristic is more conservative than the characteristic loci criterion. Other norms can also be considered. For example, the infinity norm can be defined as follows:

$$\left\|Z_S\right\|_X = \max i\left[\sum_j \left|Z_{ij}\right|\right]. \quad (39)$$

The infinity norm denotes the maximum magnitude row sum of Z_S over all possible frequencies.

$$\left\|Y_L\right\|_y = \max j\left[\sum_i \left|Z_{ij}\right|\right] \quad (40)$$

Expression (40) denotes the maximum magnitude column sum of Y_L over all possible frequencies. According to Gershgorin's theorem, each entry consists of a row–column inner production. Then,

$$\left\|Z_S\right\|_X \left\|Y_L\right\|_y < 1/2 . \quad (41)$$

The system will be stable if the previous condition is satisfied.

$$Z_S Y_L = \begin{pmatrix} a_1 & b_1 \\ c_1 & d_1 \end{pmatrix}\begin{pmatrix} a_2 & b_2 \\ c_2 & d_2 \end{pmatrix} \quad (42)$$

$$\left|\lambda_i\right| \le \sigma\left(Z_S Y_L\right) \quad (43)$$

The eigenvalues of Z_s can be expressed as follows:

$$\left|Z_s - \lambda E\right| = 0, \quad (44)$$

$$\begin{vmatrix} a_1 - \lambda & b_1 \\ c_1 & d_1 - \lambda \end{vmatrix} = 0, \quad (45)$$

$$\lambda^2 - (a_1 + d_1)\lambda + a_1 d_1 - b_1 c_1 = 0, \quad (46)$$

if:

$$\left|\lambda_1\right| < 1 \left|\lambda_2\right| < 1 \left|\lambda_1\right| + \left|\lambda_2\right| < 2 . \quad (47)$$

According to the relationship between roots and coefficients,

$$a_1 + d_1 < 2 . \quad (48)$$

Using Cauchy's inequality, the following expressions can be obtained:

$$\left|a_1\right| + \left|d_1\right| < 2, \quad (49)$$

$$\left|a_1\right| < 1 \left|d_1\right| < 1, \quad (50)$$

if:

$$\left|c_1\right| < 1 \left|d_1\right| < 1 . \quad (51)$$

The following expressions hold true:

$$\left|a_1\right|\left|d_1\right| - \left|b_1\right|\left|c_1\right| < 1, \quad (52)$$

$$|\lambda_1|<1\ |\lambda_2|<1. \tag{53}$$

The eigenvalues of Y_L can be derived similarly.

$$\|Z_S\|_M \|Y_L\|_M < 1 \tag{54}$$

The system will be stable if the previous condition is satisfied.

According to the criteria, the system will be stable if $\sigma(Z_S,\omega)\sigma(Y_L,\omega)<1$, $\|Z_S\|_M \|Y_L\|_M < 1$, or $\|Z_S\|_X \|Y_L\|_y < 1/2$. The derived stability criteria are based on system amplitude–frequency impedance parameters, rather than phase–frequency impedance parameters. Therefore, only the amplitude–frequency curve needs to be measured. The three stability criteria are necessary conditions for system stability, but are insufficient and unnecessary conditions. The most conservative criterion is the M-norm criterion, whereas the least conservative criterion is the singular criterion. Notably, the system may still be stable even if these criteria are not met. However, if one of these criteria is met, the system will definitely be stable.

IV. The Measurement Method of Harmonic Impedance

Through the previously presented analysis, the stability of the system can be easily determined by the impedance parameters of each part of the microgrid. Therefore, microgrid impedance parameter measurement has become a key issue. The basic principle of microgrid impedance measurement is to inject harmonic current with certain magnitude and frequency, such that voltage at the measuring point would be distorted accordingly. In this condition, harmonic impedance could be calculated through the distorted voltage and the injected harmonic current.

Before injecting the harmonic current, the voltage of measuring point A is defined as u_0 and the current is defined as i_0. After injection i_h, the voltage of point A turns to u_1. Harmonic voltage caused by harmonic current is $u_h = u_1 - u_0$. Then, harmonic impedance could be calculated as follows:

$$Z_h(jw) = \frac{U_h(jw)}{I_h(jw)}. \tag{55}$$

The switching capacitor method and the thyristor-controlled sub-circuit switching method have common disadvantages, that is, the injected harmonic current could not be accurately controlled and could not cover all frequency ranges, which reduced measurement accuracy. The harmonic current injection method can overcome these shortcomings. The structure is shown in Fig. 4.

In Fig. 4, the circuit is a standard two-phase bridge converter. When this circuit is applied to current injection, a current-regulated PWM method, such as hysteresis modulation or delta modulation, can be used to ensure appropriate currents. Switching frequency varies with the frequency of the square wave current. Given that we injected the square wave current, switching frequency is low. The proposed method does not require high switching frequency of the switching device. This device can also use the sweep method to measure the impedance parameters. If the measured impedance parameters are obtained by the sweep method, the switching frequency needs to be a multiple of the injected frequency to obtain a good resolution.

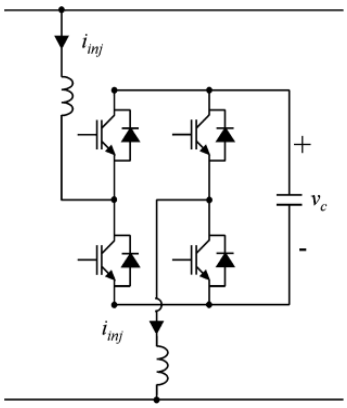

Fig. 4. Harmonic current injection method.

This harmonic injection device has only two phases, which can be applied to the AC and DC systems. The proposed methods increase the measurement speed by injecting a two-phase square wave current to the system. Compared with the sweep method, the square wave contains a large number of harmonics, which can significantly reduce measurement time. System impedance parameters could change with the operating point of the system. Reducing measurement time will increase measurement accuracy. If measurement time is long, then the measurement system impedance parameters may vary with the operating point and produce errors.

Using the proposed method to measure impedance of the AC system, an asymmetric square current disturbance is injected into the system only once. Then, the impedance matrices of the system in all interested frequency ranges can be obtained. Measurement time is only several seconds. The flowchart of measurement is shown in Fig. 5.

The detailed process is as follows: First, an asymmetric square current is injected into the system between two arbitrary phases; for example, lines a and b. Notably, current perturbations in lines a and b will have the same amplitude and opposite phase, which can be expressed as follows:

$$\begin{aligned} i_{ha} &= 0 \\ i_{hb} &= I_m i(t) \\ i_{hc} &= -I_m i(t) \end{aligned}, \tag{56}$$

where $i(t)$ is the expression of the square current. Current perturbations and the resulting voltage perturbations at a specific interface of the system can be captured by current sensors, voltage sensors, and a data acquisition card. These

Fig. 5. Flowchart of the proposed method.

perturbations can be decomposed into harmonic components by FFT analysis; taking the current perturbations as an example, they can be expressed as follows:

$$\begin{aligned} i_{ha} &= 0 \\ i_{hb} &= \sum_{k=1}^{\infty} \mathrm{I}_m\, i(\mathrm{t}) \sin(\mathrm{k}\,\omega_0\,\mathrm{t} + \varphi_k) \\ i_{hc} &= -\sum_{k=1}^{\infty} \mathrm{I}_m\, i(\mathrm{t}) \sin(\mathrm{k}\,\omega_0\,\mathrm{t} + \varphi_k) \end{aligned} \quad . \tag{57}$$

These perturbations are a series of asymmetric harmonic currents, which can be transferred to positive, negative, and zero sequence components (in this case, the zero sequence component is zero). The positive and negative sequence components can be expressed in Eqs. (58) and (59), respectively, as follows:

$$\begin{aligned} i_{ha}(1) &= \sum_{k=1}^{\infty} \mathrm{I}_{mk1} \sin(\mathrm{k}\,\omega_0\,\mathrm{t} + \varphi_{k1}) \\ i_{hb}(1) &= \sum_{k=1}^{\infty} \mathrm{I}_{mk1} \sin(\mathrm{k}\,\omega_0\,\mathrm{t} - \frac{2\pi}{3} + \varphi_{k1}) \\ i_{hc}(1) &= \sum_{k=1}^{\infty} \mathrm{I}_{mk1} \sin(\mathrm{k}\,\omega_0\,\mathrm{t} - \frac{4\pi}{3} + \varphi_{k1}) \end{aligned} \quad , \tag{58}$$

$$\begin{aligned} i_{ha}(2) &= \sum_{k=1}^{\infty} \mathrm{I}_{mk2} \sin(\mathrm{k}\,\omega_0\,\mathrm{t} + \varphi_{k2}) \\ i_{hb}(2) &= \sum_{k=1}^{\infty} \mathrm{I}_{mk2} \sin(\mathrm{k}\,\omega_0\,\mathrm{t} + \frac{2\pi}{3} + \varphi_{k2}) \\ i_{hc}(2) &= \sum_{k=1}^{\infty} \mathrm{I}_{mk2} \sin(\mathrm{k}\,\omega_0\,\mathrm{t} + \frac{4\pi}{3} + \varphi_{k2}) \end{aligned} \quad . \tag{59}$$

The positive and negative sequence currents are symmetric. After *d–q* transformation (assuming that the transfer angular frequency is the fundamental frequency ω_0), the expressions of harmonic currents and harmonic voltages can be obtained. Taking the negative sequence component of the *k*-order harmonic current and positive sequence component of *k* + 2-order component as examples, in the synchronous *d–q* coordinate, they are represented by i_{dq1} and i_{dq2}, respectively.

$$\begin{bmatrix} i_{d1} \\ i_{q1} \end{bmatrix} = \begin{bmatrix} -I_{k+1} \cos\left[(k+1)\omega_0 t + \varphi_{k1}\right] \\ I_{k+1} \sin\left[(k+1)\omega_0 t + \varphi_{k1}\right] \end{bmatrix} \tag{60}$$

$$\begin{bmatrix} i_{d2} \\ i_{q2} \end{bmatrix} = \begin{bmatrix} I_{k+2} \cos\left[(k+1)\omega_0 t + \varphi_{k2}\right] \\ I_{k+2} \sin\left[(k+1)\omega_0 t + \varphi_{k2}\right] \end{bmatrix} \tag{61}$$

i_{dq1} and i_{dq2} are linearly independent variables, which can be used to calculate the impedance matrix at frequency $(k + 1)\,\omega_0$ using Eq. (62) and combining the resulting voltages. Similarly, other impedance matrices at other frequencies can also be calculated by the same process simultaneously.

$$\begin{bmatrix} z_{dd}(\mathrm{s}) & \mathrm{Z}_{dq}(\mathrm{s}) \\ z_{qd}(\mathrm{s}) & \mathrm{Z}_{qq}(\mathrm{s}) \end{bmatrix} = \begin{bmatrix} U_{d1}(\mathrm{s}) & \mathrm{U}_{d2}(\mathrm{s}) \\ U_{q1}(\mathrm{s}) & \mathrm{U}_{q2}(\mathrm{s}) \end{bmatrix} \cdot \begin{bmatrix} I_{d1}(\mathrm{s}) & \mathrm{I}_{d2}(\mathrm{s}) \\ I_{q1}(\mathrm{s}) & \mathrm{I}_{q2}(\mathrm{s}) \end{bmatrix}^{-1} \tag{62}$$

As discussed previously, the proposed method only needs to inject current disturbance once. Then, all impedance matrices in the interested frequency ranges can be resolved. Obtaining a square current disturbance is easy, and real-time measurement performance can be improved.

V. Experimental Results

A simulation model of a microgrid operating in islanding

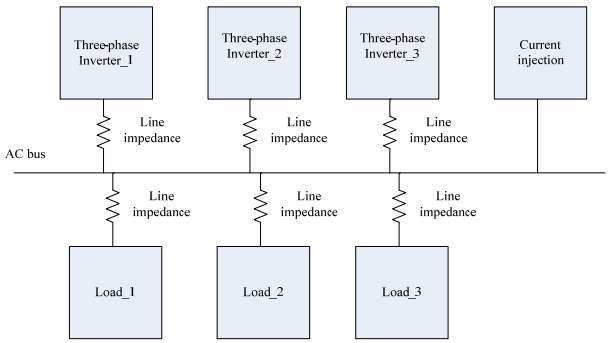

Fig. 6. Simulation model.

(a) Harmonic current injection device.

(b) Microgrid experimental platform.

Fig. 7. Experimental platform.

mode is developed using PSCAD (Fig. 6), which contains three inverters and three loads. The inverters are controlled as voltage sources, and the droop control is used to share power to the loads. The simulation parameters should be consistent with the experimental platform to verify the accuracy of the measurement results.

The harmonic current injection device, as shown in Fig. 7(a), contains a computer, injection module, current and voltage sensors, and a DSP control system. Three-phase voltages and two-phase currents on the source and load sides are captured to obtain the impedance parameters. Then, these data are transformed to the synchronous reference frame before source impedance and load admittance can be extracted. Fig. 7(b) shows a laboratory microgrid experimental platform, which contains microgrid control cabinets, inverters, and load. The microgrid control cabinets are used to control microgrid connection and cut off the

TABLE II
PARAMETERS OF THE INVERTER

Parameter	Value	Parameter	Value
K_{vp}	0.071	K_{ip}	0.045
K_{vi}	25	K_{ii}	120
U_{DC}	200 V	R_f	1 Ω
L_f	0.62 mH	R_v	2.5 Ω
C_f	35 μF	L_v	15 mH

TABLE III
PARAMETERS OF THE INDUCTION MACHINE

r_{s1} = 3.53 Ω	P_1 = 4	r'_{r1} = 3.34 Ω
L'_{lr1} = 4.53 mH	L_{M1} = 36.34 mH	L_{ls1} = 7.01 mH
r_{s2} = 4.38 Ω	P_2 = 2	r'_{r2} = 4.63 Ω
L'_{lr2} = 4.56 mH	L_{M2} = 138.34 mH	L_{ls2} = 12.5 mH

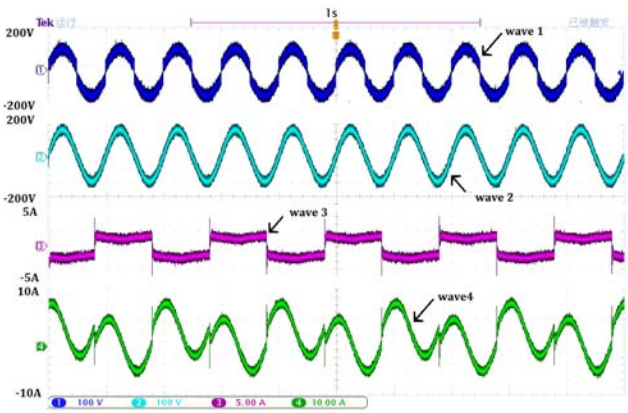

Fig. 8. Time domain test results.

power grid. In this study, the microgrid operates in islanding mode. Droop control is used to share power to the loads. Three parallel inverters are used in this experimental platform. The parameters for inverters 1 and 2 are the same, as shown in Table I. The parameters for inverter 3 are different, as shown in Table II. The inverters are used to connect sources to the microgrid. The loads are two different induction motors and a resistive load. The parameters are listed in Table III.

Fig. 8 shows the time domain test results, with three waves. Waveform 1 represents the bus voltage after square wave current injection. Waveform 2 represents the bus voltage before square wave current injection. Waveform 3 is the square wave current. Waveform 4 represents the bus current after square wave current injection.

One practical issue is the attenuation of the injected harmonic current. Theoretically, the square wave current contains rich orders of harmonics. By injecting a low-frequency current, all impedance parameters can be obtained. However, in high-frequency current, the harmonic current will become small, which leads to inaccurate measurement results. Thus, the frequency of the square wave current is different. If the low-frequency impedance parameters of the system need to be measured, then a low-frequency square wave current must be injected into the

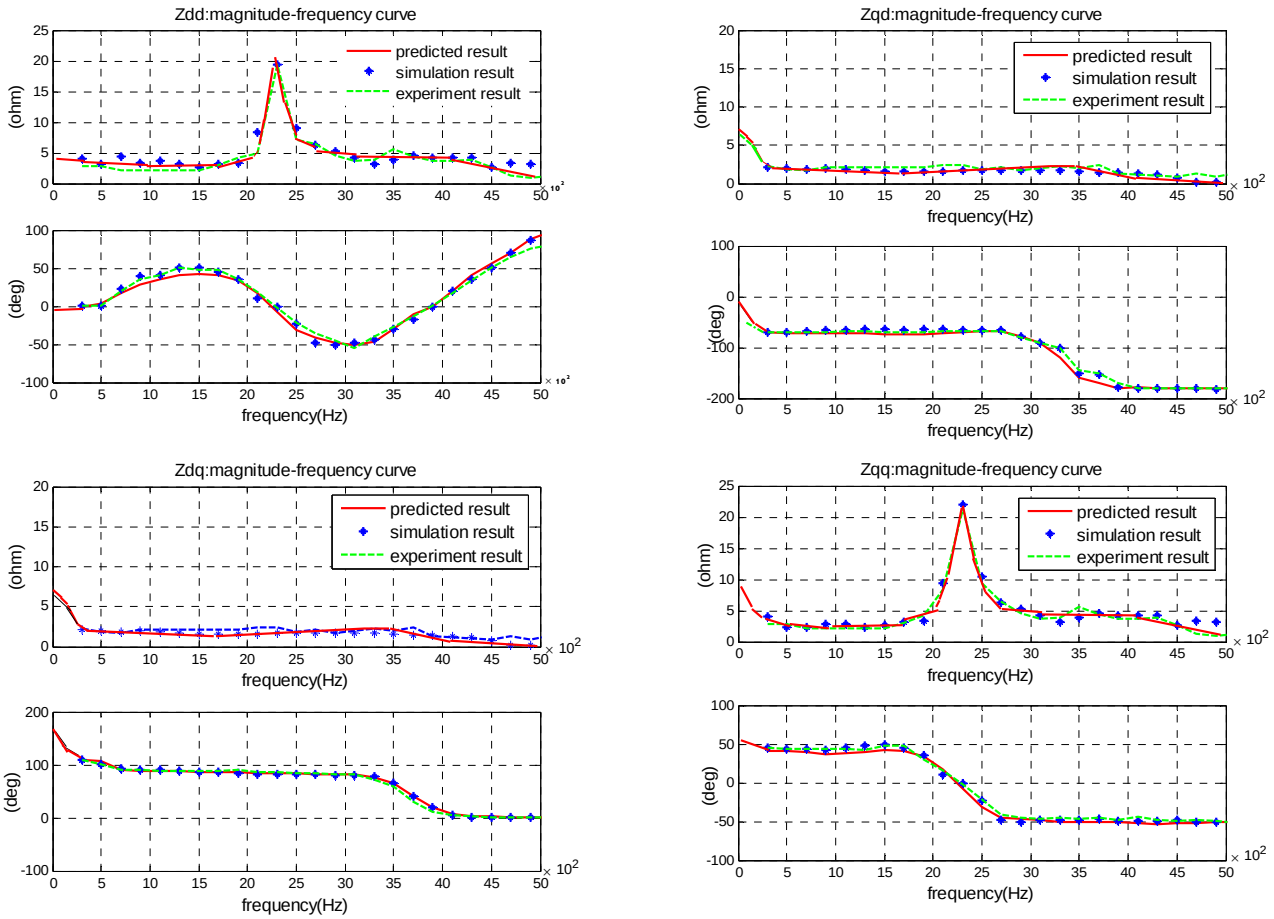

Fig. 9. Comparison of the source impedance results of the AC system.

system. If the high-frequency impedance parameters of the system need to be measured, then a high-frequency square wave current must be injected into the system. Low-frequency harmonic currents have greater effect on the system than high-frequency harmonic currents. Therefore, this study provides the current and voltage waveforms of the system after injecting the square wave current at low frequency. As shown in the waveform, significant differences are observed in the bus current before and after injection. However, the change of the bus voltage is not obvious. Therefore, harmonic current injection does not have a significant effect on system operations. In addition to injection frequency, the amplitude of the harmonic currents also affects system operations. Harmonic currents with a large magnitude have a more significant effect on system operations, although they facilitate impedance measurements. In Fig. 9, source impedances obtained from experiments, simulations, and calculations (predicted result) are compared.

Fig. 9 shows the discrepancies among the measured, calculated, and simulation curves in certain frequencies. The reason is that the system itself contains a number of harmonic currents in these frequencies. Overall, the measured amplitude–frequency and phase–frequency curves are consistent with the calculated and simulation curves.

Fig. 10 shows the load admittance contrast figures of the experimental, simulation, and calculated results (predicted results).

Fig. 10 shows that the measured amplitude–frequency curves are quite close to the calculated and simulation curves at the low-frequency part. However, obvious deviation appears at the high-frequency part of the phase–frequency curves. That is, measurement accuracy is significantly affected because the magnitude of high-frequency components in the square wave current would decrease to almost zero.

Overall, the measured amplitude–frequency and phase–frequency curves are consistent with the calculated and simulation curves. The contrasting results indicate that the harmonic current injection method is suitable for measuring the harmonic impedance of the microgrid.

This harmonic injection device has only two phases, which can also be applied to DC systems. The proposed methods increase measurement speed by injecting a two-phase square wave current to the system. A laboratory prototype of the system shown in Fig. 11 was assembled to validate the proposed method in DC systems. The system consists of a

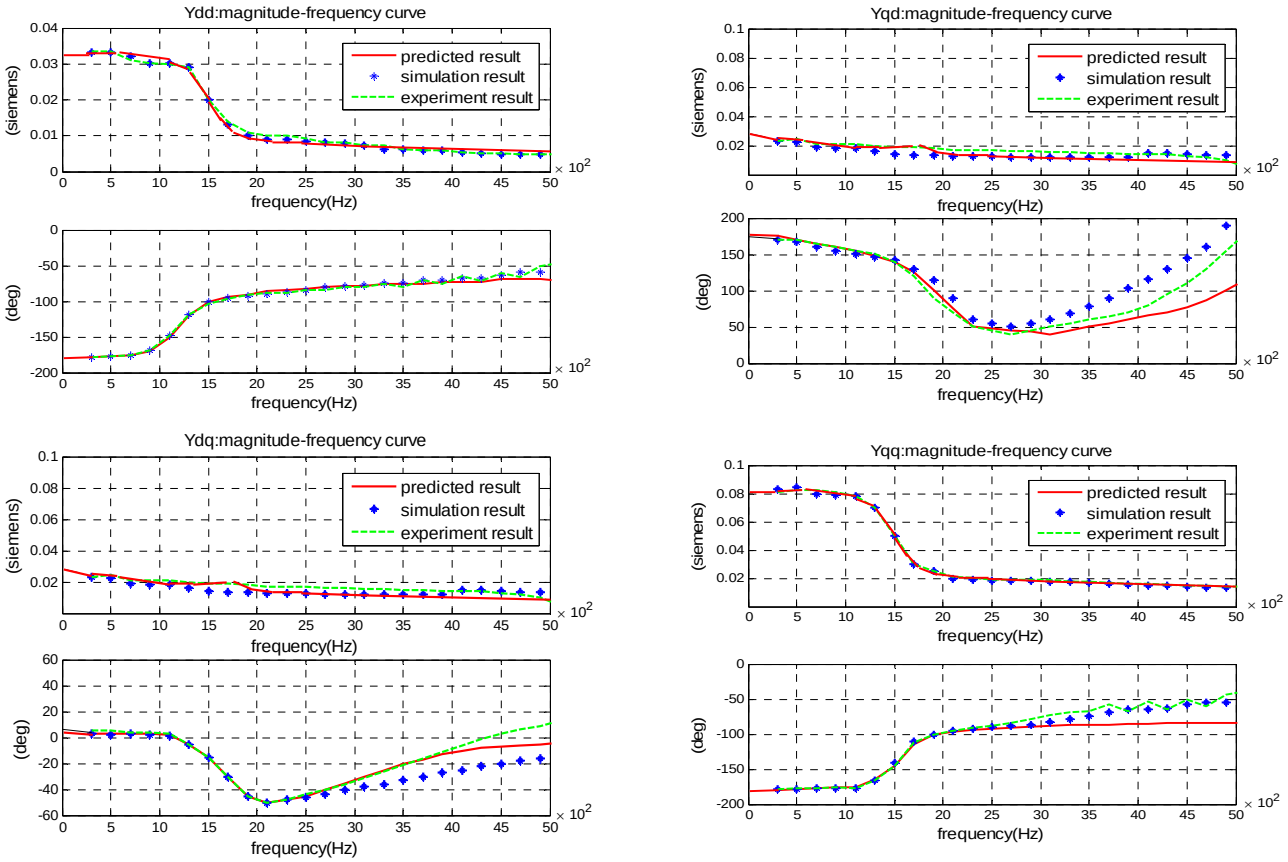

Fig. 10. Comparison of the load admittance results of the AC system.

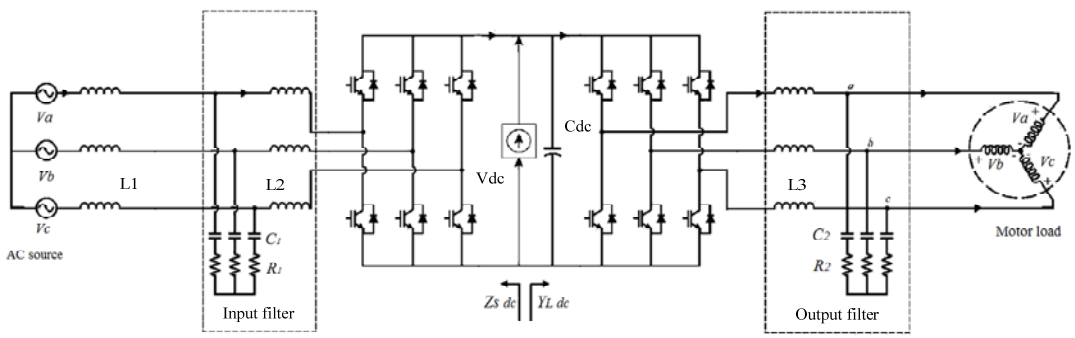

Fig. 11. Example system for DC impedance measurement demonstration.

back-to-back rectifier/inverter feeding an induction motor load. PWM filters are added between the AC source and rectifier and between the inverter and motor load. The AC source has an inductance of L_1 = 0.36 mH and a line-to-neutral terminal voltage of 120 V. Both PWM filters have parameters of $R_1 = R_2 = 9.12\ \Omega$, $L_2 = L_3 = 1.1$ mH, and $C_1 = C_2 = 6.95$ μF. The DC-link capacitance is C_{DC} = 5,000 μF.

For DC impedance measurement, square wave currents are injected at the output of the rectifier (before the DC-link capacitor). Source impedance and load admittance at the DC system are shown in Fig. 12.

The switching capacitor method, sweep method, and proposed method are used to test the impedance parameters of the same DC system to verify the superiority of the proposed method. Impedance parameters in Fig. 12 represent ZS and YL, as shown in Fig. 11. Based on Fig. 12, the square wave current method curves are quite close to the sweep method curves in most frequencies. In the high-frequency section, certain deviations are observed between the results of the two methods. This finding is due to harmonic current attenuation in the high frequency. Overall, only a slight difference is observed in the accuracy of the two methods. The credible range of measurement can meet practical application needs, which could verify the effectiveness of the proposed method. The switching capacitor method curves

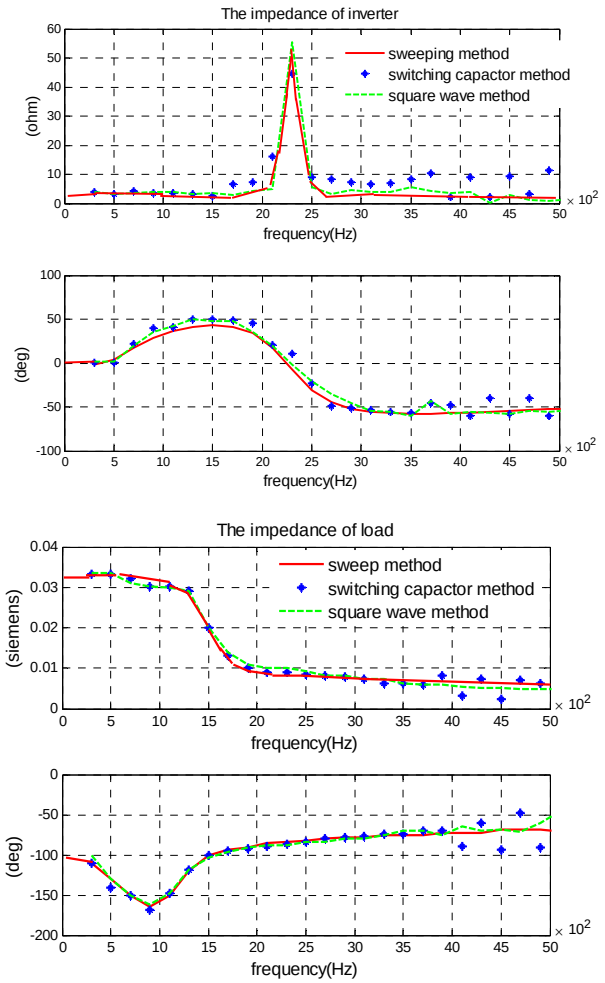

Fig. 12. The results of the three measurement methods in the DC system.

exhibit obvious deviation with the sweep method curves. The reason is that the harmonic currents injected by the switching capacitor method have been missing at certain frequencies, not only at high frequencies but also at low frequencies. The accuracy of the measurement results could be seriously affected. Compared with the parameters of the high-frequency section, the parameters of the low-frequency section are more extensively used and more significant.

The measurement time and accuracy of these three methods are compared in Table IV to compare the advantages and disadvantages of several methods more clearly. The calculated impedance parameters are used as a standard value and compared with the impedance parameters obtained by other methods. Measurement accuracy is calculated as follows:

$$\left|\text{measurement value} - \text{standard value}\right| / \left|\text{standard value}\right| \text{‰}.$$

The proposed new approach performs better in terms of accuracy than the switching capacitor method. Compared with the sweep method, the proposed approach significantly

TABLE IV
THE MEASUREMENT TIME AND ACCURACY OF THREE METHODS

	Sweep method	Square wave current method	Switching capacitor method
Measurement time	20 min	2 min	0.5 min
Measurement accuracy	91%	89%	65%

reduces measuring time while still preserving high measurement accuracy. In this study, the operating state of the system does not change. However, a long measurement time will affect measurement accuracy when the operating state of the system changes. Therefore, in a system with frequently changing working state, the measurement accuracy of the sweep method is lower than that of the proposed method. Compared with the sweep method, the proposed method also has advantages in switching frequency. The proposed approach significantly reduces switching frequency because of square wave current injection. The switching frequency of the sweep method is 50–200 times more than that of the proposed method. A low switching frequency will reduce the requirements for devices, which also means that our proposed method is suitable for high voltages. Overall, this new approach includes the advantages of the traditional method.

Fig. 13 shows the dynamic response test results where the load is stepped from light load to heavy load in the microgrid to verify the stability criterion derived in Section III. In a stable system, as shown in Fig. 13(a), the bus voltage of the system appears to fluctuate during the load step, but quickly restores stability. In an unstable system, as shown in Fig. 13(b), the bus voltage fluctuates during the load step and the system cannot restore stability. The Nyquist criterion and derived criterion experiment are also compared when the system is stable and unstable (Fig. 14). Impedances were computed using the measurement results in the AC bus microgrid. According to the criteria, the system will be stable if $\sigma(Z_S,\omega)\sigma(Y_L,\omega)<1$ (Criterion 1) or $\|Z_S\|_M \|Y_L\|_M < 1$ (Criterion 2) or $\|Z_S\|_X \|Y_L\|_y < 1/2$ (Criterion 3). The most conservative criterion is the $\|Z_S\|_X \|Y_L\|_y < 1/2$ criterion, whereas the least conservative criterion is $\sigma(Z_S,\omega)\sigma(Y_L,\omega)<1$ criterion. If these criteria are not satisfied, then the system may still be stable and the complete generalized Nyquist plot can be used to predict stability. However, if one of these criteria is met, then the system is stable. Therefore, these AC criteria could be used in most applications where a robust stability margin is required. In Fig. 14(a), the Nyquist curve is obtained from the dynamic response stable system. The figure also shows that the curve does not surround the (−1, 0) point. The curves in Fig. 14(c)

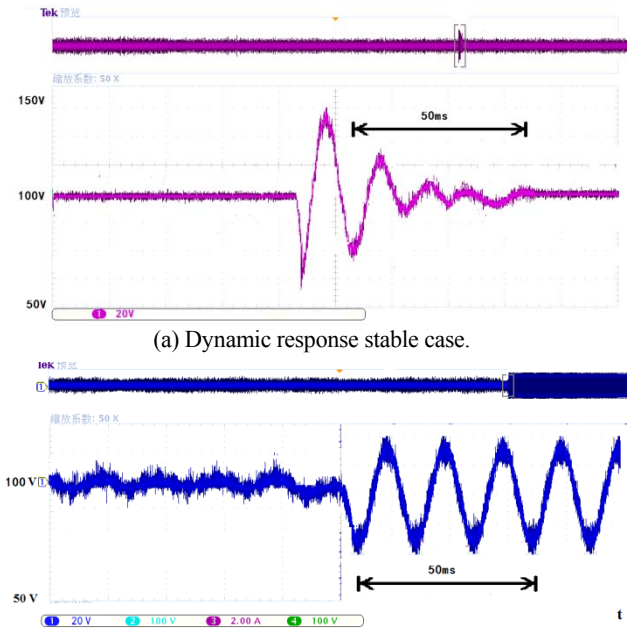

(a) Dynamic response stable case.

(b) Dynamic response unstable case.

Fig. 13. Dynamic response test results.

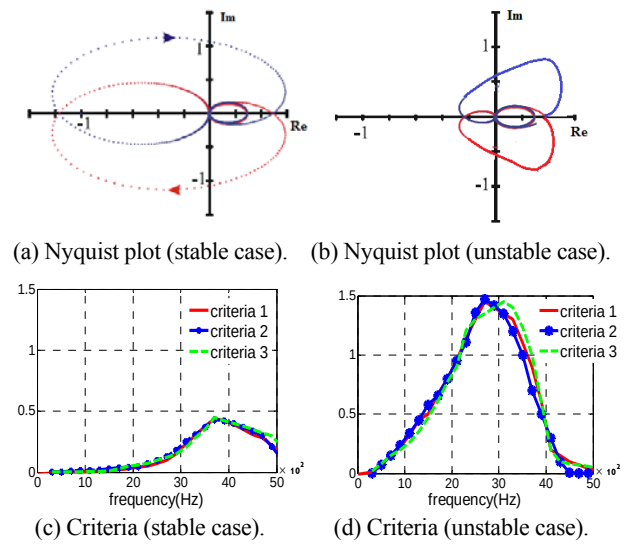

(a) Nyquist plot (stable case). (b) Nyquist plot (unstable case).

(c) Criteria (stable case). (d) Criteria (unstable case).

Fig. 14. Stability criteria and Nyquist plots.

obtained from the dynamic response stable system show that only Criterion 2 predicts system instability. This criterion is the most restrictive criterion. Therefore, the criteria predicted that the system is stable. In Fig. 14(b), the Nyquist curve is obtained from the dynamic response unstable system. The figure shows that the curve surround the (−1, 0) point and the system is unstable. Criteria 1, 2, and 3 are indications of system instability, as shown in Fig. 14(d); the curves are obtained from the dynamic response unstable system. In this case, all criteria predict instability. The results match the Nyquist curve results.

VI. Conclusions

This study proposes a novel technique for measuring microgrid impedance. By injecting an unbalanced line-to-line square wave current between two lines of the AC system, all impedance information can be determined simultaneously. Compared with the sweeping method, the proposed approach significantly reduces measuring time while still maintaining high measurement accuracy. Experiments showed that the actual measurement results are accurate and are consistent with those from theoretical calculation and simulation. The impedance criteria are further deduced for easy use. The proposed stability criteria only need to calculate the system amplitude–frequency curves, not the phase–frequency curves. The accuracy of the phase–frequency curves is not guaranteed because of the decreased amplitude of the injected square wave currents at high frequency.

With the measured data, the Nyquist criterion and the proposed criterion are compared when the system is stable and unstable. The results show that system stability has a significant relationship with the impedance parameters. Thus, the effectiveness of the proposed method is well verified.

References

[1] S. V. Iyer, M. N. Belur, and M. C. Chandorkar, "A generalized computational method to determine stability of a multi-inverter microgrid," *IEEE Trans. Power Electron.*, Vol. 25, No. 9, pp. 2420- 2432, Sep. 2010.

[2] N. Pogaku, M. Prodanovic, and T. C. Green, "Modeling, analysis and testing of autonomous operation of an inverter based microgrid," *IEEE Trans. Power Electron.*, Vol. 22, No. 2, pp. 613-625, Mar. 2007.

[3] E. Barklund, N. Pogaku, and M. Prodanovic, "Energy management in autonomous microgrid using stability-constrained droop control of inverters," *IEEE Trans. Power Electron.*, Vol. 23, No. 5, pp. 2346-2352. Sep. 2008.

[4] S. Anand and B. Fernandes, "Reduced order model and stability analysis of low voltage DC microgrid," *IEEE Trans. Ind. Electron*, Vol. 60, No.11, pp. 5040-5049, Nov. 2013.

[5] M. A. Hassan, M. A. Abido, "Optimal design of microgrids in autonomous and grid-connected modes using particle swarm optimization," *IEEE Trans. Power Electron*, Vol. 26, No. 3, pp. 755-769, Mar. 2011.

[6] J. M. Guerrero, L. G. de Vicuna, J. Matas, M. Castilla, J. Miret, "A wireless controller to enhance dynamic performance of parallel inverters in distributed generation system," *IEEE Trans. Ind. Electron.*, Vol. 19, No. 5, pp. 1205-1213, Sep. 2004,

[7] A. Emadi, A. Khaligh, C. H. Rivetta, and G. A. Williamson, "Constant power loads and negative impedance instability in automotive systems: Definition, modeling, stability and control of power," *IEEE Trans. Veh. Technol.*, Vol. 55, No. 4, pp. 1112-1125, Jul. 2006.

[8] X. Feng, J. Liu, and F. C. Lee, "Impedance specifications for stable dc distributed power systems," *IEEE Trans. Power Electron.*, Vol. 17, No. 2, pp. 157-162, Mar. 2002.

[9] J. Liu, X. Feng, F. C. Lee, and D. Borojevich, "Stability margin monitoring for dc distributed power systems via current/voltage perturbation," in *Proc. IEEE Appl. Power Electron. Conf.*, pp. 745-751, 2001.

[10] P. Xiao, G. K. Venayagamoorthy, and K. A. Corzine, "A novel impedance measurement technique for power electronic systems," in *Proc. IEEE Power Electron. Spec. Conf*., pp. 955-960, 2007.
[11] J. Sun, "Input impedance analysis of single-phase PFC converters," *IEEE Trans. Power Electron*., Vol. 20, No. 2, pp. 308-314, Mar. 2005.
[12] Y. Panov and M. Jovanovic, "Practical issues of input/output impedance measurements in switching power supplies and application of measured data to stability analysis," in *Proc. IEEE Appl. Power Electron. Conf,* Vol. 2, pp. 1339-1345, 2005.
[13] R. D. Middlebrook, "Input filter consideration in design and application of switching regulators," *IEEE Industry Applications Society Annual Meeting*, 1976.
[14] J. J. Liu, X. G. Feng, and F. C. Lee, "Stability margin monitoring for DC distributed power systems via perturbation approaches," *IEEE Trans. Power Electron*, Vol. 18, No. 6, pp. 1254-1261, Nov. 2003.
[15] S. D. Sudhoff, S. F. Glover, P. T. Lamm, D. H. Schmucker, and D. E. Delisle, "Admittance space stability analysis of power electronic systems," *IEEE Trans. Aerosp. Electron. Syst.*, Vol. 36 No. 3, pp. 965-973, Jul. 2000.
[16] J. Sun, "Impedance-based stability criterion for grid-connected inverters," *IEEE Trans. Power Electron*, Vol. 26, No. 11, pp. 3075-3078, Nov. 2011.
[17] Y. Xiao, J. C. Maun, H. B. Mahmoud, T. Detroz, and S. Do, "Harmonic impedance measurement using voltage and current increments from disturbing loads," *Harmonics and quality of power, 2000 proceedings.ninth international conference*, pp. 220-225, 2000.
[18] H. Yang, P. Prrotte, E. De Jaeger, and A. Robert, "A Harmonic emission levels of industrial loads-statistical estimation," *CIGER Report 36-306*, p. 8, 1996.
[19] M. J. Bridgeman, R. E. Morrison, and S. B. Tenakoon, "Measurement of harmonic impedance on an LV system utilizing power capacitor switching and consequent predictions of capacitor induced harmonic distortion," *Harmonics and quality of power,1998.proceedings.8th international conference*, pp. 1141-1145, 1998.
[20] X. Feng, Z. Ye, K. Xing, and F. C. Lee, "Individual load impedance specification for a stable dc distributed power system," in *Proc. IEEE Appl. Power Electron. Conf.*, pp. 923-929, 1999.
[21] X. Feng and F. C. Lee, "Online measurement on stability margin of dc distributed power system," in *Proc. IEEE Appl. Power Electron. Conf.*, pp. 1190-1196, 2000.
[22] L. Hou, B. Liu, H. Shi, H. Yi, and F. Zhuo, "New techniques for measuring islanded microgrid impedance characteristics based on current injection," in *2014 International Power Electronics Conference (IPEC2014)*, 2014.
[23] L. Hou, H. Shi, Z. Yang, and F. Zhuo, "Harmonic impedance calculation and measurement for an islanded microgrid," *ECCE Asia Downunder (ECCE Asia)*, *IEEE*, 2013.
[24] H. Shi, Z. Yang, X. Yue, L. Hou, and F. Zhuo, "Calculation and measurement of harmonic impedance for a microgrid operating in Islanding mode," *Power Electronics and Motion Control Conference (IPEMC)*, *2012 7th International*, 2012.
[25] J. C. Vsquez Quintero, J. M. G. Zapata, M. Savaghevi, and R. Teodorescu, "Modeling, analysis, and design of stationary reference frame droop controlled parallel three-phase voltage source inverters, " *IEEE Trans. Ind. Electron*., Vol. 60, No.4, pp. 1271-1280, Apr. 2013.
[26] W. Yao, M. Chen, J. Matas, J. M. Guerrero, and Z. Qian, "Design and analysis of the droop control method for parallel inverters considering the impact of the complex impedance on the power sharing," *IEEE Trans. Ind. Electron*., Vol. 58, No. 2, pp. 576-588, Feb. 2011.
[27] J. He and Y. W. Li, "Analysis, design, and implementation of virtual impedance for power electronics interfaced distributed generation," *IEEE Trans. Ind. Electron*., Vol. 47, No.6, pp. 2525-2538, Nov. 2011.

Lixiang Hou was born in Xi'an, China. He received his B.S.E.E. and M.S.E.E. degrees from North China Electrical Power University, Beijing, China in 2008 and 2011, respectively. He is currently working toward his Ph.D. degree at Xi'an Jiaotong University. His current research interests include power electronics, power quality, and microgrids.

Fang Zhuo was born in Shanghai, China on May 1962. He received his B.S. degree in Automatic Control from Xi'an Jiaotong University in 1984. Then, he joined Xi'an Jiaotong University. He received his M.S. and Ph.D. degrees in Automation and Electrical Engineering from Xi'an Jiaotong University in 1989 and 2001, respectively. In 2004, he worked as a visiting scholar in Nanyang Technological University. He was an associate professor in Xi'an Jiaotong University in 1996 and a full-time professor in Power Electronics and Drives in 2004. Then, he was employed as a supervisor of Ph.D. students. He is also the associate dean of the Faculty of Industry Automation. Dr. Zhuo's research interests include power electronics, power quality, active power filter, reactive power compensation, and inverters for distributed and power generation. He is the author or coauthor of more than 160 publications; more than 30 papers were indexed by SCI, EI, and ISTP in his research fields. He is also the coauthor of two handbooks. He is the key finisher of 4 projects sponsored by the National Natural Science Foundation of China and more than 40 projects in cooperation with companies from the industry. He is the owner of four provincial-level and ministerial-level science and technology advancement awards and four patents. Professor Zhuo is a member of IEEE, China Electro-technical Society, Automation Society, and Power Supply Society. In addition, he is the power quality professional chairman of the Power Supply Society in China.

Hongtao Shi was born in Hebei, China in 1984. He received his B.S. and M.S. degrees in electrical engineering from Ningxia University, Ningxia, China in 2008 and 2011, respectively. He received his Ph.D. degree in electrical engineering from Xi'an Jiaotong University, Xi'an, China in 2015. He is currently a member of Beifang University of Nationalities, Ningxia, China. His research interests include modeling and control of distributed generation systems.